SCIENCE CHINA
Earth Sciences

Human activity and climate change triggered the expansion of rocky desertification in the karst areas of Southwestern China

Chaojun CHEN, Daoxian YUAN, Hai CHENG[4], Tsailuen YU[4], Chuanchou SHEN[4], R. Lawrence EDWARDS[8], Yao WU[1], Siya XIAO[1], Jian ZHANG[1], Tao WANG[1], Ran HUANG[1], Ziqi LIU[10], Tingyong LI[10] and Junyun LI[10]

Citation: SCIENCE CHINA Earth Sciences; doi: 10.1007/s11430-020-9760-7

View online: https://engine.scichina.com/doi/10.1007/s11430-020-9760-7

Published by the Science China Press

SCIENCE CHINA
Earth Sciences

•RESEARCH PAPER•

https://doi.org/10.1007/s11430-020-9760-7

Human activity and climate change triggered the expansion of rocky desertification in the karst areas of Southwestern China

Chaojun CHEN[1,2,3], Daoxian YUAN[1,2], Hai CHENG[4], Tsailuen YU[5,6], Chuanchou SHEN[5,6,7], R. Lawrence EDWARDS[8], Yao WU[1], Siya XIAO[1], Jian ZHANG[1,9], Tao WANG[1], Ran HUANG[1], Ziqi LIU[10], Tingyong LI[3*] & Junyun LI[1,2†]

[1] *Chongqing Key Laboratory of Karst Environment, School of Geographical Sciences, Southwest University, Chongqing 400715, China;*
[2] *Key Laboratory of Karst Dynamics, MNR; Guangxi, Institute of Karst Geology, Chinese Academy of Geological Sciences, Guilin 541004, China;*
[3] *Yunnan Key Laboratory of Plateau Geographical Processes & Environmental Changes, Faculty of Geography, Yunnan Normal University, Kunming 650500, China;*
[4] *Institute of Global Environmental Change, Xi'an Jiaotong University, Xi'an 710049, China;*
[5] *High-precision Mass Spectrometry and Environment Change Laboratory (HISPEC), Department of Geosciences, Taiwan University, Taipei 10617, China;*
[6] *Research Center for Future Earth, Taiwan University, Taipei 10617, China;*
[7] *Global Change Research Center, Taiwan University, Taipei 10617, China;*
[8] *Department of Earth Sciences, University of Minnesota, Minneapolis, MN 55455, USA;*
[9] *Environnements et Paléoenvironnements Océaniques et Continentaux (EPOC), UMR CNRS 5805, Université de Bordeaux, Pessac 33600, France;*
[10] *School of Karst Science, Guizhou Normal University, Guiyang 55001, China*

Received July 22, 2020; revised February 23, 2021; accepted March 19, 2021; published online August 9, 2021

Abstract It is conducive to the sustainable development of human beings in karst regions to research the mechanism of karst rocky desertification (KRD) expansion. Whether the large-scale KRD in southwestern China is caused by climate change or human activities is still controversial. In this study, the evolution of the KRD in southwestern China over the past 2000 years was reconstructed through the high-precision $\delta^{13}C$ record of stalagmites from Shijiangjun (SJJ) Cave, Guizhou Province, China. The $\delta^{13}C$ of the stalagmites from SJJ Cave exhibited heavy values from the Medieval Warm Period (MWP) to the Little Ice Age (LIA). Furthermore, the $\delta^{13}C$ records of other stalagmites and tufa from southwestern China also showed the same significant heavy trend. Because the stalagmite $\delta^{13}C$ could record the change of ecological environment, it indicated that the consistent change of the stalagmites $\delta^{13}C$ may record the process of KRD expansion in the karst regions of southwestern China. During the MWP, the stronger Asian summer monsoon and the northward movement of the rain belt led to a dry period in southwestern China and a wet period in northern China. In contrast, it was wet in southwestern China and dry in northern China during the LIA. In addition, after the Jing-Kang event (JK event, AD1127) occurred at the end of the Northern Song dynasty, the political and economic center of China migrated to southern China for the first time, which changed the population distribution pattern of larger population in the north and smaller population in the south. Therefore, the expansion of KRD in southwestern China was exacerbated in the MWP due to the change of climate in southwestern China, the migration of a large number of people, wars, the large-scale reclamation of arable land, and the cultivation of large areas of crops.

Keywords Karst rocky desertification, Jing-Kang event, Stalagmite $\delta^{13}C$ record, Medieval Warm Period, Little Ice Age

* Corresponding author (email: cdlity@163.com)
† Corresponding author (email: jxljy@swu.edu.cn)

Citation: Chen C, Yuan D, Cheng H, Yu T, Shen C, Edwards R L, Wu Y, Xiao S, Zhang J, Wang T, Huang R, Liu Z, Li T, Li J. 2021. Human activity and climate change triggered the expansion of rocky desertification in the karst areas of Southwestern China. Science China Earth Sciences, 64, https://doi.org/10.1007/s11430-020-9760-7

1. Introduction

Karst rocky desertification (KRD) is the process by which the surface vegetation and soil in a karst area change to almost no vegetation and soil, producing a rocky landscape (Yuan, 1997; Appendix Figure S1 online). KRD is the most serious ecological and environmental problem in the karst regions of China and around the globe (Bai et al., 2011; Jiang et al., 2014). In particular, the karst regions in southwestern China cover a total area of 7.5×10^5 km^2, accounting for 43% of the total area of southwestern China (Zeng et al., 2016). These areas have fragile ecosystems, a prominent contradiction between human beings and land, and serious soil erosion and KRD (Figure 1). All of these factors have seriously affected the sustainable development of the regional economy (Zhang et al., 2019). Over the last few decades, the KRD in southwestern China has been effectively controlled, but this region will face the risk of KRD again, or even the expansion of KRD due to global warming and frequent extreme climate events (Jiang et al., 2014; Guo et al., 2015). The intensity of human activities (such as population growth, agricultural expansion, and wars) began to change the natural KRD process in karst regions as early as 3000–4000 year BP (Gams, 1991; Yassoglou, 2000; Liu et al., 2011). At the end of the Northern Song dynasty (AD1127), the army of the Jin Dynasty conquered Kaifeng City (Figure 1a), the capital of the Northern Song Dynasty, and captured the Huizong and Qinzong emperors of the Song Dynasty, resulting in the fall of the Northern Song Dynasty, which is known as the Jing-Kang event (JK event) in history (Dai and Bie, 2015). After the JK event, the political and economic center of ancient Chinese civilization migrated to Lin'an City (now Hangzhou City) south of the Yangtze River, resulting in a population migration from northern to southern China (Figure 1a). Subsequently, the large-scale migration of the Chinese population to southern China changed the natural evolution of the ecological environment (Wei, 1986; Wu, 2000; Dai and Bie, 2015). Therefore, it is of great significance to explore the influence of human activities and climate change on KRD during this period.

Cave stalagmites have become an important geological tool for the reconstruction of changes in the paleoclimate and paleoenvironment (Wang et al., 2001, 2005; Fleitmann et al., 2003; Yuan et al., 2004; Wang et al., 2017; Cheng H et al., 2019). The accurate U-Th dating of stalagmites and their continuous and high-resolution records not only provide a reference for global paleoclimate changes (Wang et al., 2001, 2005; Fleitmann et al., 2003; Yuan et al., 2004; Wang et al., 2017; Cheng H et al., 2019) but also offer a great deal of evidence for the evolution of human civilizations caused by climate change, such as the Maya civilization, the Indus civilization, the Mesopotamian civilization, and the ancient Chinese civilization (Polyak and Asmerom, 2001; Zhang et al., 2008; Kathayat et al., 2017; Sinha et al., 2019). However, most studies have focused on the stalagmite δ^{18}O and laminae proxy, and few studies have focused on the δ^{13}C records of stalagmites. Moreover, the δ^{13}C of stalagmites is controlled by the climatic and non-climatic factors outside the cave (Liu et al., 2016; Li et al., 2018; Cheng K et al., 2019), and there may be regional hydrological differences, so the details of each record are different (Tan et al., 2015; Liu et al., 2016; Li et al., 2018). However, compared with the δ^{18}O records of stalagmites, the δ^{13}C records are more sensitive to the changes in the ecological environment outside the cave (Zhang et al., 2015; Liu et al., 2016). In this study, the stalagmite δ^{13}C records for southwestern China were used to explore the influence of human activities and climate change on KRD in karst regions over the past 2000 years.

2. Study area and samples

Shijiangjun Cave (SJJ) (26.2°N, 105.5°E, 1300 m a.s.l.) is located in Anshun City, Guizhou Province, southwestern China (Figure 1). It is located on the gradual slope of the eastern part of the Yunnan-Guizhou Plateau. Guizhou is the center of the karst area in southern China, and the karst area accounts for 92.5% of the total area of Guizhou Province. The KRD is the most serious in this area (Figure 1c; Bai et al., 2011). SJJ Cave is located in the Middle and Upper Triassic, intermediate to thick limestone dolomite (Li et al., 2016). The landform type is a peak cluster depression. The top of the cave is covered with about 100 m of bedrock, and shrub vegetation is well-developed. The natural entrance of the cave is 2 m high and 1.5 m wide, and the entire length of the cave is about 500 m. The airflow and exchange between the cave and the outside are very limited, and the cave temperature remains at around 15°C throughout the year (Li et al., 2016). Mean annual precipitation is about1400 mm (Li et al., 2021). The regional climate is strongly affected by the Asian summer monsoon, and the water vapor in the rainy season mainly comes from the Indian Ocean and the Pacific Ocean (Figure 1).

This study is based on two stalagmites, SJJ-300 and SJJ7, which were collected from SJJ Cave. Stalagmite SJJ7 is cylindrical overall, with three slight deviations along the

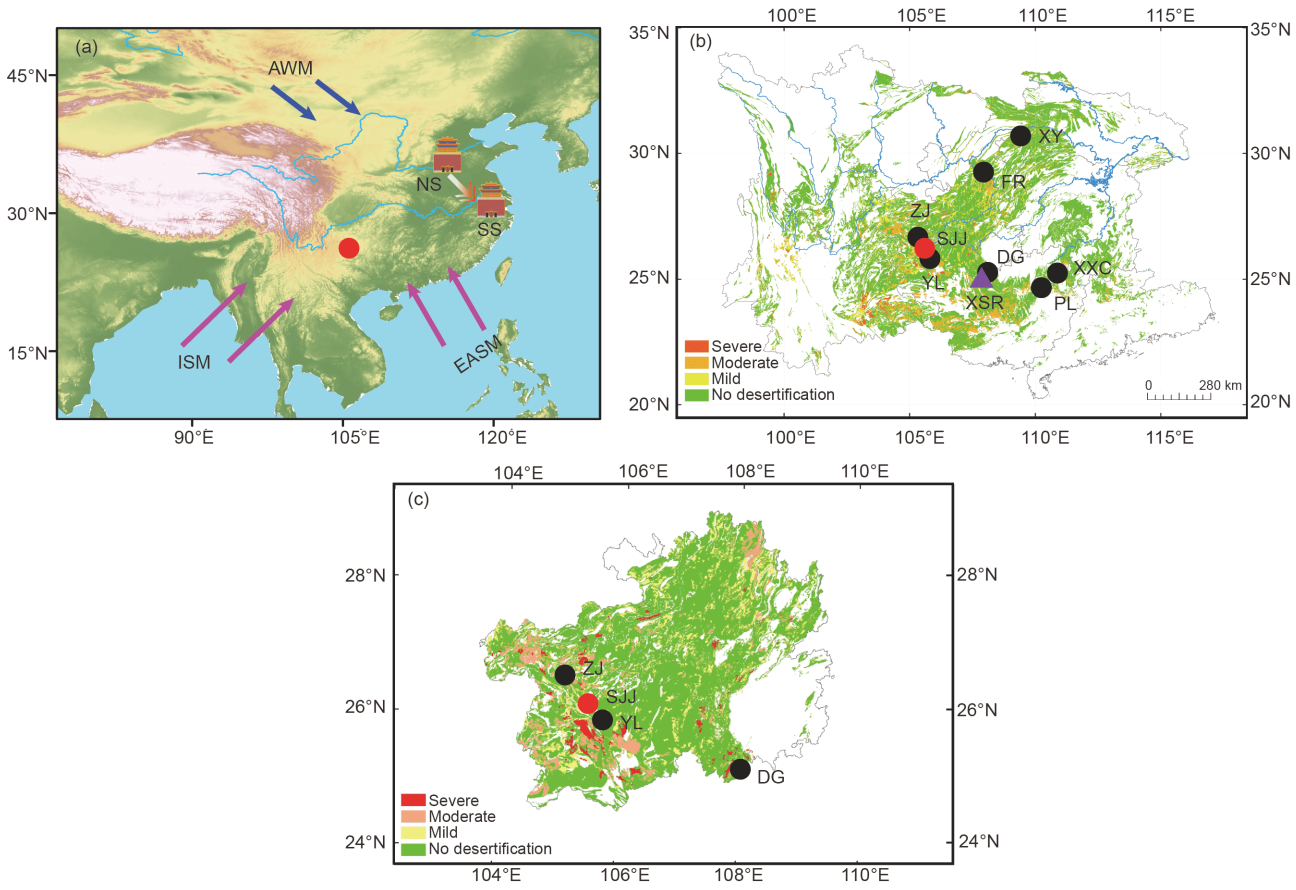

Figure 1 Location of Shijiangjun Cave (SJJ) and other paleoclimate records. (a) Location of SJJ Cave and schematic diagram of the Asian summer monsoon. The purple arrows indicate the Indian summer monsoon (ISM) and the East Asian summer monsoon (EASM), and the blue arrow indicates the Asian winter monsoon (AWM). NS indicates Kaifeng (the capital of the Northern Song dynasty), and SS indicates Lin'an (the capital of the Southern Song dynasty). After the JK event, the capital of the Song dynasty moved from Kaifeng to Lin'an. (b) The distribution and grade of the karst rocky desertification (KRD) in southwestern China. (c) The distribution and grade of the KRD in Guizhou Province. The red dot indicates SJJ Cave (in this study), and the black dots indicate the locations of other records (Table 1) and Panlong Cave (PL) (Yin et al., 2019). The purple triangle is the location of the tufa from the Xiangshui River (Liu et al., 2011). The KRD data are from Li et al. (2008) and Bai et al. (2011).

growth axis, and experienced continuous deposition. The total length of the stalagmite along its growth axis is about 254 mm, and there are 11 mm of calcite deposits 30–19 mm from the top (Figure 2a). The growth axis of stalagmite SJJ-300 shifted 6 times, and the total length of stalagmite SJJ-300 along its growth axis is 330 mm (Figure 2b).

3. Methods

Parallel to the growth layers in SJJ7 and SJJ-300, powder sub-samples (10–50 mg) were collected from the polished profile of the stalagmite using a dental drill with a diameter of 1 mm for the U-Th age testing. A total of 47 and 55 dating samples were collected from stalagmites SJJ7 and SJJ-300, respectively. The sampling locations are shown in Figure 2. The U and Th were separated using the standard chemical procedures described by Edwards et al. (1987), Shen et al. (2012), and Cheng et al. (2013). The ^{230}Th ages of the SJJ-300 were determined in the High-Precision Mass Spectrometry and Environment Change Laboratory (HISPEC), Department of Geosciences, Taiwan University, China. The ^{230}Th age of SJJ7 was determined in the Isotope Laboratory of the Institute of Global Environmental Change, Xi'an Jiaotong University, China (44/47) and the Age Laboratory of Taiwan University (3/47) using a multi-collector inductively coupled plasma mass spectrometer (MC-ICP-MS, Neptune-Plus) with a statistical error of ±2σ. The decay constant of ^{230}Th is 9.1705×10^{-6} yr^{-1} (Cheng et al., 2013), that of ^{234}U is 2.82206×10^{-6} yr^{-1} (Cheng et al., 2013), and that of ^{238}U is 1.55125×10^{-10} yr^{-1} (Jaffey et al., 1971). The corrected ^{230}Th ages assume an initial ^{230}Th/^{232}Th atomic ratio of $(4.4\pm2.2)\times10^{-6}$. These are the values for material in secular equilibrium with the bulk Earth ^{232}Th/^{238}U value of 3.8.

The isotope sub-samples were collected using a dental drill with a diameter of 0.5 mm from the polished profile along

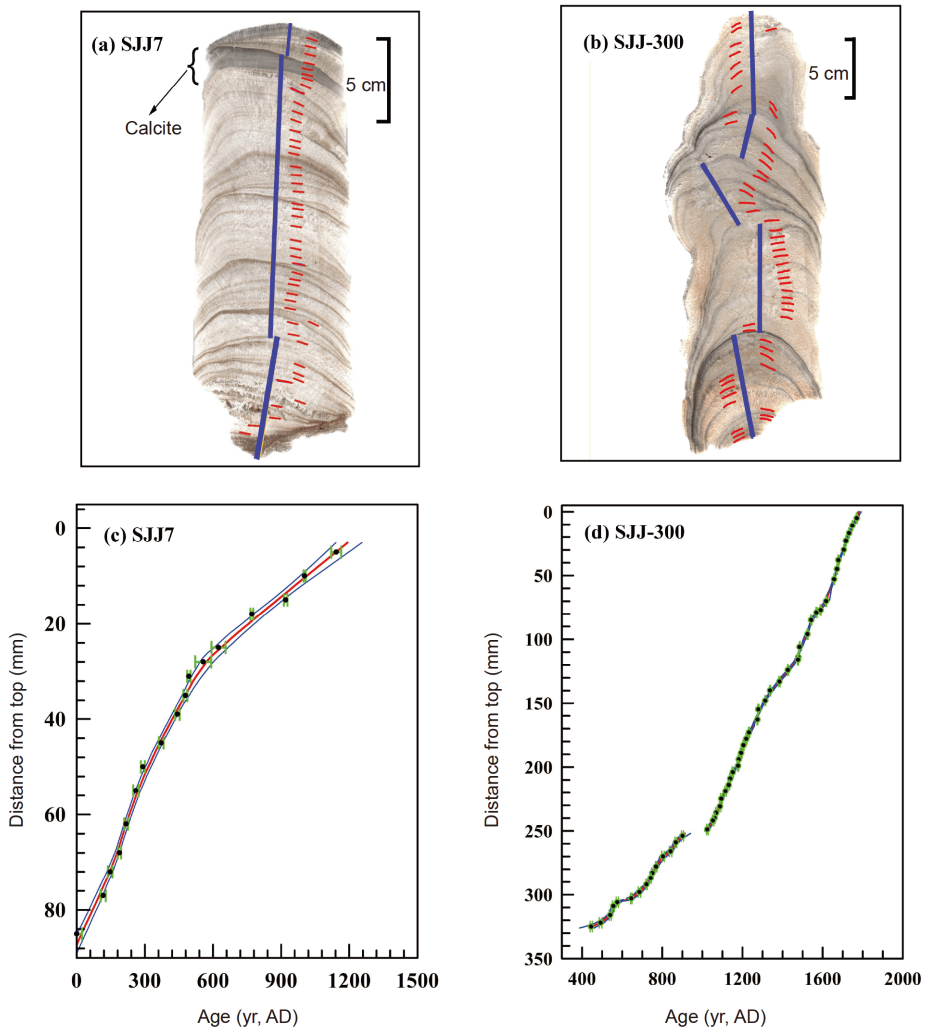

Figure 2 The samples and age models for stalagmites SJJ7 and SJJ-300. (a) and (b) are profile pictures of stalagmites SJJ7 and SJJ-300, respectively. Stalagmite SJJ7 contains an 11 mm calcite deposit 30–19 mm from the top. The blue solid line indicates the oxygen and carbon isotope sampling path, and the short red transverse line indicates the age sampling locations. (c) and (d) show the simulated chronological models for stalagmites SJJ7 and SJJ-300 created using the Mod-Age software, respectively (Hercman and Pawlak, 2012).

the central growth axis of the stalagmite (Figure 2). Each sub-sample was drilled at intervals of 0.25 mm. The $\delta^{13}C$ analyses of the stalagmite samples were performed using a Delta V Plus isotope ratio mass spectrometer equipped with a Kiel IV Carbonate Device at the Geochemistry and Isotope Laboratory of Southwest University. One standard sample (SWU-1) was tested with every seven samples. The results are reported relative to the Vienna-Pee Dee Belemnite standard (V-PDB). The analysis error ($\pm 1\sigma$) is less than 0.06‰ for $\delta^{13}C$ (Li T Y et al., 2011).

4. Results

The ^{230}Th dating results are presented in Appendix Table S1 online. The ^{238}U concentrations of stalagmites SJJ-300 and SJJ7 are 8031–50743 and 385–47542 ppb (1 ppb=1 μg kg^{-1}), respectively. The dating errors of the two stalagmites were less than 6 and 59 years, respectively, and the average dating errors were ±3.4 and ±14.1 years, respectively. The model ages of the two stalagmites were established using the Mod-Age software and the dating results (Hercman and Pawlak, 2012). The simulation results show that stalagmite SJJ7 grew from BC1158 to AD1256 (Figure 2c) and stalagmite SJJ-300 grew from AD380 to AD1782, but there were two hiatus from AD 578 to 631 (305.25 mm in depth) and from AD924 to AD1023 (250 mm in depth) (Figure 2d).

The changes in the $\delta^{13}C$ records of stalagmites SJJ7 and SJJ-300 in the same growth period were similar (Figure 3a) and are significantly correlated (R=0.31, $p \leq 0.01$), with resolutions of 3.6 and 1 yr, respectively. When the same mother liquor was deposited as aragonite and calcite, the carbon isotope fractionation coefficients were different, and the $\delta^{13}C$ in the calcite was lighter than that in the aragonite (Tarutani

et al., 1969; Scroxton et al., 2017). According to the research of Fohlmeister et al. (2018), the $\delta^{13}C$ of stalagmite SJJ7 was corrected by adding 1.07‰±0.41‰ in the calcite section. The results show that the corrected $\delta^{13}C$ record did not change the overall trend of the record (Appendix Figure S2 online). The corrected $\delta^{13}C$ of stalagmite SJJ7 ranged from −6.1‰ to 1.1‰, with an average of −3.8‰ and an increase of 5.9‰ from the MWP to the LIA. The average $\delta^{13}C$ value of stalagmite SJJ7 was −4.0‰ and −0.4‰ during AD0–1127 and AD1128–1256, respectively. The $\delta^{13}C$ range of stalagmite SJJ-300 is −8.1‰ to −1.6‰, with an increase of 6.5‰ from the MWP to the LIA. The average $\delta^{13}C$ value was −5.5‰ and −4.3‰ during AD380–1125 and AD1127–1782, respectively. The values of $\delta^{13}C$ of SJJ-300 and SJJ7 are different, which may be caused by the differences in the thickness of upper bedrock, soil thickness, vegetation, drip rate and residence time of difference drip site in same cave (Li and Li, 2018; Li et al., 2018). However, after the JK event, the $\delta^{13}C$ of both stalagmites (SJJ-300 and SJJ7) was significantly heavier (Figure 3a). The coincident changes of stalagmite $\delta^{13}C$ in the same cave, at least, indicate a common driving mechanism (Liu et al., 2016).

5. Discussion

5.1 The $\delta^{13}C$ of stalagmites indicated the evolution of KRD

The carbon in the stalagmite is mainly from the CO_2 in the overlying soil and the carbonate in the bedrock (Bergel et al., 2017; Cheng K et al., 2019). The ventilation of the cave, the dissolution degree of the bedrock, the type and density of vegetation, the microbial activity in the soil, the prior calcite precipitation (PCP) in the karst surface zone, and the evaporation and degassing of the drip water all affected the changes in the $\delta^{13}C$ of the stalagmites (Fairchild et al., 2006; Tan et al., 2015; Li et al., 2018). These influencing factors are all controlled by the hydrological environment of the cave (Li et al., 2018), and the differences in the environment often lead to differences in the $\delta^{13}C$ of cave stalagmites in different regions (Liu et al., 2016). However, the $\delta^{13}C$ values of stalagmites within a large region are closely related to climatic factors (precipitation and temperature) (Li T Y et al., 2011; Li et al., 2018), and climate change will lead to the same hydrological environment in a large region. Therefore, the $\delta^{13}C$ values of stalagmites from different caves within a large region will have similar environmental implications.

The $\delta^{13}C$ of the stalagmite may reflect the changes in vegetation coverage. The $\delta^{13}C$ was lighter when there was more vegetation under humid climate conditions and was heavier when there was less vegetation (Li et al., 2017). The CO_2 produced by the respiration of plants and biological activity in the soil may be the main factor affecting the $\delta^{13}C$ of the stalagmites (Bergel et al., 2017; Li et al., 2018). During the cold-dry season, the vegetation growth rate was limited, the productivity of CO_2 in the soil from microorganisms was reduced, the dripping speed slowed, and the degasification of the CO_2 in the dripping water increased, which increased the $\delta^{13}C$ values of the stalagmites (Zhao et al., 2015, 2017). The modern monitoring results show that the $\delta^{13}C$ in dripping water of cave is controlled by surface precipitation and temperature and the CO_2 in the soil, resulting in heavier $\delta^{13}C$ values in the winter and spring and lighter $\delta^{13}C$ values in the summer and autumn (Li and Li, 2018).

Climate change and human activity (population migration, agricultural production, deforestation, etc.) can lead to the destruction of surface vegetation and the degradation of soil productivity, then trigger KRD (Li et al., 2018; Wang et al., 2020). Soil CO_2 concentration from the respiration of plants and biological activity decrease because KRD results in lower vegetation coverage and thinner soil thickness (Li and Li, 2018; Li et al., 2018). In addition, the water storage capacity of soil decrease, infiltration flow rapidly through the soil, and lower CO_2 soil dissolve into ground water (Li and Li, 2018). Above these factors can lead to the $\delta^{13}C$ of stalagmites toward heavier (Figure 4a). Furthermore, the Chinese government has promulgated relevant laws (Law of the People's Republic of China on Forest, Law of the People's Republic of China on Grasslands, Law of the People's Republic of China on Water and Soil Conservation) and measures (Ecological project of returning farmland to forest and grassland) to protect the ecological environment since AD1984 (Wang et al., 2020; Luo et al., 2021). KRD in Southwest China has been effectively controlled and gradually restored (Luo et al., 2021). The $\delta^{13}C$ of the stalagmites in Panlong Cave and Xinya Cave in southwestern China from AD1970 to AD2009 showed that the $\delta^{13}C$ gradually became lighter with the restoration of the ecological environment in karst regions (Figure 4b) (Li et al., 2017; Yin et al., 2019). Therefore, the $\delta^{13}C$ of stalagmites in karst regions can indicate the evolution of KRD (Zhang et al., 2004; Liu et al., 2011; Li et al., 2018; Yin et al., 2019).

5.2 The expansion of KRD in southwestern China increased after the JK event

After the JK event, the $\delta^{13}C$ values of stalagmites SJJ7 and SJJ-300 gradually became heavier and remained heavier throughout the LIA (Figure 3a). In the same area (Figure 1), the $\delta^{13}C$ of stalagmites from ZJ Cave dramatically became heavier during the JK event (Figure 2b). After AD1100, the $\delta^{13}C$ values of a stalagmite from Furong Cave in Chongqing quickly increased from −2.6‰ to −0.9‰ (Figure 3c) (Li H C et al., 2011). During the same period, the $\delta^{13}C$ values of a stalagmite from Xinya Cave in Chongqing became significantly heavier, even heavier than in the latter part of the

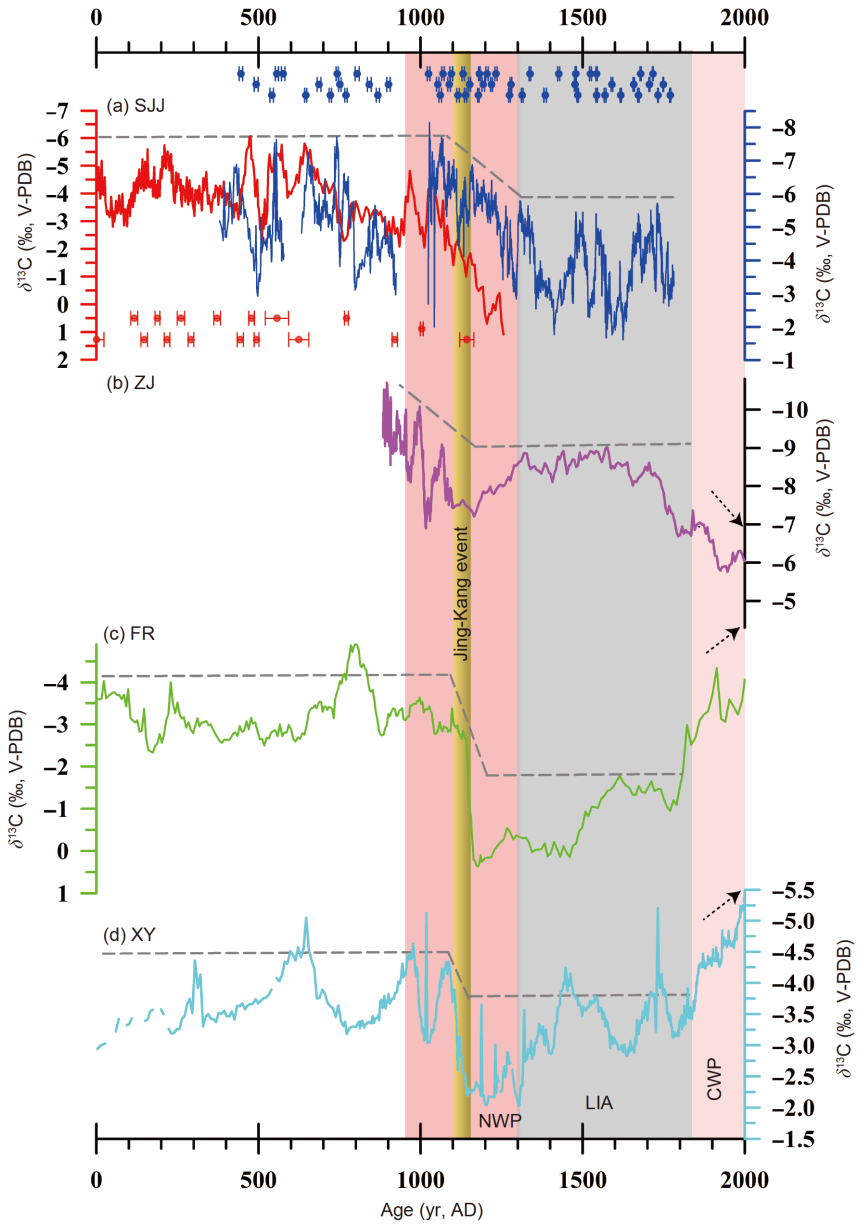

Figure 3 The $\delta^{13}C$ records of stalagmites SJJ7 and SJJ-300 and other stalagmites from southwestern China over the past 2000 years. (a) The $\delta^{13}C$ records of stalagmite SJJ7 (red curve) and stalagmite SJJ-300 (blue curve). The red and blue error bars are the dating points and the dating errors of stalagmite SJJ7 and stalagmite SJJ-300, respectively; (b) the $\delta^{13}C$ record of a stalagmite from Zhijin Cave (ZJ) (Kuo et al., 2011); (c) the $\delta^{13}C$ record of a stalagmite from Furong Cave (FR) (Li H C et al., 2011); and (d) the $\delta^{13}C$ record of a stalagmite from Xinya Cave (XY) (Li et al., 2017). MWP, LIA, and CWP are the Medieval Warm Period, the Little Ice Age, and the Current Warm Period, respectively. The grey dotted lines indicate the variation trend. The black dashed arrow shows the change of the stalagmite $\delta^{13}C$ during the CWP.

LIA (Figure 3d) (Li et al., 2017). Moreover, the increase in the magnitude of the stalagmite $\delta^{13}C$ in Xiangshui Cave in Guizhou Province in AD1100 was far greater than that over the past 6,000 years (Zhang et al., 2004). In addition, the $\delta^{13}C$ of stalagmites from Yelang Cave, and Dongge Cave in the same area even reached the magnitude of the Younger Dryas event and the Heinrich event (Table 1) (Kuo et al., 2011; Liu et al., 2016; Zhao et al., 2017). Studies of tufa from the Xiangshui River in Guizhou Province showed that the $\delta^{13}C$ exhibited an abrupt stepped change around AD1270 (Liu et al., 2011). This abrupt positive excursion in the stalagmite $\delta^{13}C$ records did not just occur in a single cave after about AD1100, but it was a common feature in the karst regions of southwestern China (Table 1). This abrupt change in each record was explained by the weakening of the summer monsoon (Liu et al., 2016), the massive deforestation caused by the population migration (Zhao et al., 2015), the reduction of vegetation coverage, the increase in C4 plants (Li et al., 2017), the enhancement of agricultural production (Zhang et al., 2004), and the import of C4 crops

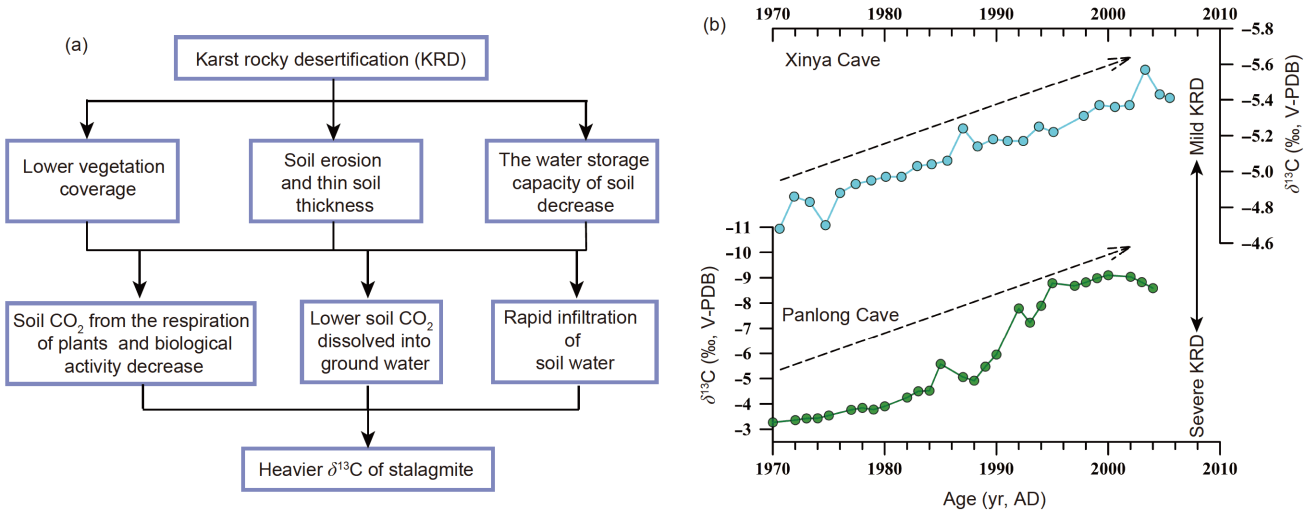

Figure 4 The relationship between KRD and the stalagmite $\delta^{13}C$. (a) Conceptual model between KRD and the stalagmite $\delta^{13}C$; (b) the stalagmite $\delta^{13}C$ value of Xinya Cave (Li et al., 2017) and Panlong Cave (Yin et al., 2019) gradually became lighter with the recovery of KRD since AD1980.

Table 1 The increased magnitude of the $\delta^{13}C$ of stalagmite and tufa in southwestern China from the MWP to the LIA

Site	Abbreviation	Location	Duration (AD)	Proxies	The increased magnitude (‰)	Impact factors	Reference
Shijiangjun Cave	SJJ	26.20°N, 105.50°E 1300 m	950–1350	Stalagmite	5.9 and 6.5	Climate change and Human activity	This study
Xinya Cave	XY	30.75°N, 109.47°E 1250 m	1000–1400	Stalagmite	2.5	Vegetation coverage decreased and human activity increased	Li et al., 2017
Furong Cave	FR	29.23°N, 107.90°E 480 m	1150–1500	Stalagmite	4.4	Not discussed	Li et al., 2011
Yelang Cave	YL	26.04°N, 105.74°E 1285 m	1300–1900	Stalagmite	8.0	C4 plant and human activity increased	Zhao et al., 2017
Zhijin Cave	ZJ	26.35°N, 105.33°E 1300 m	990–1800	Stalagmite	3.3	Deforestation and Population migration	Kuo et al., 2011
Xiangshui Cave	XSC	25.48°N, 111.88°E 400 m	1000–1500	Stalagmite	7.0	C4 plant and human activity increased	Zhang et al., 2004
Xiangshui River	XSR	25.47°N, 107.88°E 700 m	1000–1270	Tufa	1.9	Importing of C4 crops	Liu et al., 2011
Dongge Cave	DG	25.28°N, 108.08°E 680 m	1000–1400	Stalagmite	1.6	Weak summer monsoon	Liu et al., 2016

(Liu et al., 2011). Although these explanations were only based on a single record, they may indicate the enhancement of human activities and the rapid expansion of KRD in the karst regions of southwestern China. Although there are discrepancy of these stalagmite $\delta^{13}C$ records (Figure 3), they can reflect that different intensity of human activities led to different KRD levels during JK event.

5.3 Precipitation patterns in the Asian monsoon region during the MWP and the LIA

A large number of paleoclimate reconstruction records all indicate that climate change had occurred on abnormal two way in hundred years over the past two millennia, i.e., during the MWP and the LIA (Wang et al., 2005; Zhang P Z et al., 2008; Chen et al., 2015; Zhao et al., 2020). Although the onset and end time of the MWP and the LIA are still slightly controversial, a large number of records indicated that there was a significant change in the Asian summer monsoon (East Asian summer monsoon and Indian summer monsoon) from AD950–1300 to AD1300–1850 (Appendix Table S2 online), while the summer monsoon region of southwestern China exhibited a pattern opposite that of northern China (Figure 5). A comparison of the paleoclimate reconstructions obtained using multiple indicators, such as stalagmites, lakes, peat, pollen, loess, and historical data, was conducted (Appendix Table S2 online), and the results are as follows: (1) During the MWP, the climate in southwestern China was relatively dry and that in the north and east was humid due to the influence of the East Asian summer monsoon (EASM) (Figure 5a). The climate in the northern part of the Indian summer monsoon (ISM) region was humid (Figure 5a). (2)

During the LIA, the climate in southwestern China was humid, and that in northern and northeastern China was relatively dry (Figure 5b). The climate in the northern part of the Indian monsoon region was dry (Figure 5b). These results are similar to those of other paleoclimate integrations and paleoclimate simulations (Appendix Table S3 online). The results of paleoclimatic simulations showed that during the MWP, the ISM moved north, resulting in a humid climate in the north and an extremely arid climate in the central ISM region. The ISM weakened during the LIA (Polanski et al., 2014).

During the MWP (LIA), the temperature increased (decreased) in the Northern Hemisphere, and the temperature gradient increased (decreased) in both Hemispheres (Liu et al., 2014). Thus, the EASM and the ISM strengthened (weakened), and the rain belt moved northward (southward) (Liu et al., 2014), resulting in an increase (decrease) in precipitation in the northern parts of the EASM and ISM regions (Zhao et al., 2020). In addition, the strong El Niño event during the MWP caused the western ascending branch of the Walker circulation in the low-latitude tropical Pacific Ocean to move eastward, resulting in a decrease in precipitation in the southern part of the Chinese monsoon region (Yan et al., 2011; Tan et al., 2019; Duan et al., 2020). Meanwhile, El Niño may have promoted the development of extreme positive phases of the Indian Ocean Dipole (IOD) (Abram et al., 2020). During the positive phase of the IOD, the sea surface temperature (SST) of the Eastern Indian Ocean decreases and the precipitation in Southeast Asia decreases due to the influence of subsidence airflow (Abram et al., 2020).

Historical documents reveal that droughts and floods in China exhibited different distribution patterns in the different cold and warm climate backgrounds over the past 2000 years (Zheng et al., 2014). During the warm periods from AD1000 to AD1100 and from AD1190 to AD1290, there were always droughts in southwestern China, and it was wet in eastern China for a long period of time (Zheng et al., 2014). Around AD1126, the average temperature in China became significantly lower (Zhang, 1991). In AD1111, Taihu Lake was completely frozen, so that the "vehicles were able to pass over the ice, and all of the litchis in Fuzhou were frozen to death" (Zhang, 1991). From AD1329 to AD1353, Taihu Lake froze two more times, which was described as "The ice is several feet thick, so that people can walk on the ice, and the citruses in Dongting Lake are almost frozen to death" (Zhang, 1991). From AD1483 to AD1513, Taihu Lake, Poyang Lake, and Dongting Lake frequently froze, and the surface of the small tributary rivers in the Yangtze River basin froze many times in the winter (Zhang, 1991). However, floods were frequent in the summer in the Yangtze River basin (Zhang Q et al., 2008). All of these historical records demonstrate that abrupt climate changes occurred during this period.

The temperature records for the Northern Hemisphere and China reveal that the MWP was not a stable warm period, but the temperature was significantly lower in the LIA (Figure 6a) (Kobashi et al., 2012). After AD1100, the temperature suddenly decreased in China, and then, China entered the LIA after a short warm period of about 70 years (Figure 6b) (Ge et al., 2013). During the MWP, the precipitation in southwestern China decreased, leading to the opening of cracks and tunnels in the upper part of the cave, prolonging the duration of the infiltration water, and strengthening the PCP and CO_2 degassing (Tan et al., 2015; Liu et al., 2016; Li et al., 2018). As a result, the $\delta^{13}C$ of the stalagmites from SJJ Cave became gradually heavier after AD1100 (Figure 6c). Although the climate in southwestern China became wet during the LIA (Figure 5b), the $\delta^{13}C$ of stalagmite SJJ-300 remained heavy, and the $\delta^{13}C$ records of other stalagmites and tufa from southwestern China were also heavy (Table 1). From the MWP to the LIA, there was no significant change in the CO_2 concentration of the atmosphere (Figure 6d). However, the total population of China in AD1125 was 4.4 times that in AD960 (Figure 6e), so increased human activities might have caused a significant change in the ecological environment in southwestern China.

5.4 Relationship between human activities and KRD

As is well known, social events, such as population migration, economic fluctuations, war, and even the rise and fall of dynasties, are closely related to climate changes (Fang et al., 2015). During the two Song dynasties, the population grew rapidly (Zhao, 1988). The population of China exceeded 100 million during the Northern Song dynasty, and the population increased rapidly in southwestern China (Zhao, 1988; Yang, 1995; Wu, 2000; Zhang and Peng, 2012). There was a reduction in the grain yield in AD1100, which increased the famine index, and the northern nomads moved southward (Fang et al., 2015; Lan et al., 2020). During the JK event (~AD1127), wars took place in northern and southern China for many years, resulting in a sharp decrease in the total population and the migration of about 5 million people from the north to the south (Wu, 2000, 2001; Zhang and Peng, 2012). After the wars ended, southwestern China became one of the regions with the fastest population growth during the Song dynasty from AD1078 to AD1162 (Wu, 2000). In the first year of Jiaxi in the Song dynasty (AD1237), the Yuan army attacked Sichuan on a large scale for 50 years, resulting in the death of 1.4 million people (Wu, 2000). During the Zhongtong in the Yuan dynasty (AD1260–1264), there were wars in southwest China (Lan, 1997). Then, a large number of military immigrants moved into the Wujiang River valley to construct extensive military defense lines and wage war against the armies of Jin and Mongolia from

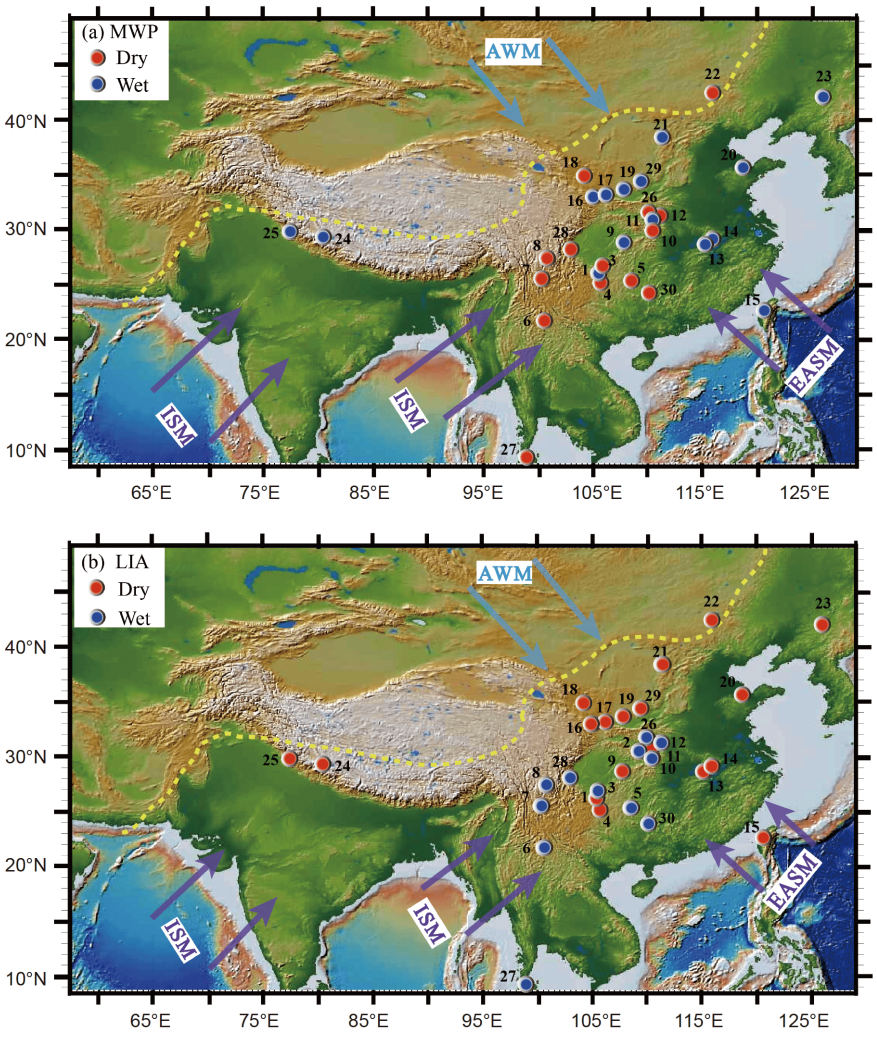

Figure 5 The change of climate in the Asian monsoon region. (a) Dry and humid patterns of the Asian monsoon region during the MWP. (b) Dry and humid patterns of the Asian monsoon region during the LIA. The red dot represents dry, and the blue dot represents wet. See Appendix Table S2 online for the information for each record. The purple arrows indicate the ISM and EASM, and the blue arrow indicates the AWM. The yellow dashed line indicates the boundary of modern Asian summer monsoon (Sun et al., 2019). The abbreviations MWP, LIA, AWM, ISM, and EASM are defined in Figures 1 and 3.

AD1127 to AD1162 (Zhang and Peng, 2012). From the 26th year of Hongwu to the 4th year of Hongzhi in the Ming dynasty (AD1393–1491), the population of Sichuan increased from more than 1.4 million to more than 2.6 million (Guo, 1988). From the end of Hongwu to the beginning of Wanli (AD1398–1573), the total cultivated area in Sichuan increased from 11.5×10^4 to 20.5×10^4 km^2 (Guo, 1988). Since the Song dynasty, the populations of Shanxi, Jiangxi, Hunan, and Sichuan have continuously moved into Guizhou, resulting in rapid population growth in Guizhou (Wei, 1986; Li, 1990). From the first year of Tianbao in the Tang Dynasty to the 33rd year of Qianlong in the Qing dynasty (AD742–1768), the registered population of Guizhou increased from about 0.16 million to 3.44 million (Wei, 1986; Li, 1990). Moreover, the failure of the northern war after JK event, the government of Song Dynasty began to strengthen the economic construction of southwestern China (Dong, 2015). The government mainly developed tea, salt, horse trade and exploited minerals to promote the development of southwestern China (Liang, 2004). However, conflicts of economic and cultural resulted in frequent rebellion in southwestern China (Zhang, 2004). For example, because most of the ethnic minorities lived in mountainous areas of southwestern China, the non-native cut down a lot of trees and built roads, which made the ethnic minorities lose their natural barriers and caused conflicts (Zhang, 2004). In the second year of Longxing in the Song dynasty (AD1164), relevant measures were issued to alleviate the contradiction between the ethnic minorities and the government, including providing cattle and promoting cattle farming technology (Zhang, 2002).

In addition, compared with the period from AD0 to AD1000, the total population of China experienced a stepwise increase from the late MWP to the LIA (Figure 6e). First, the population migration during the Song and Yuan Dynasties changed the pattern of the population distribution

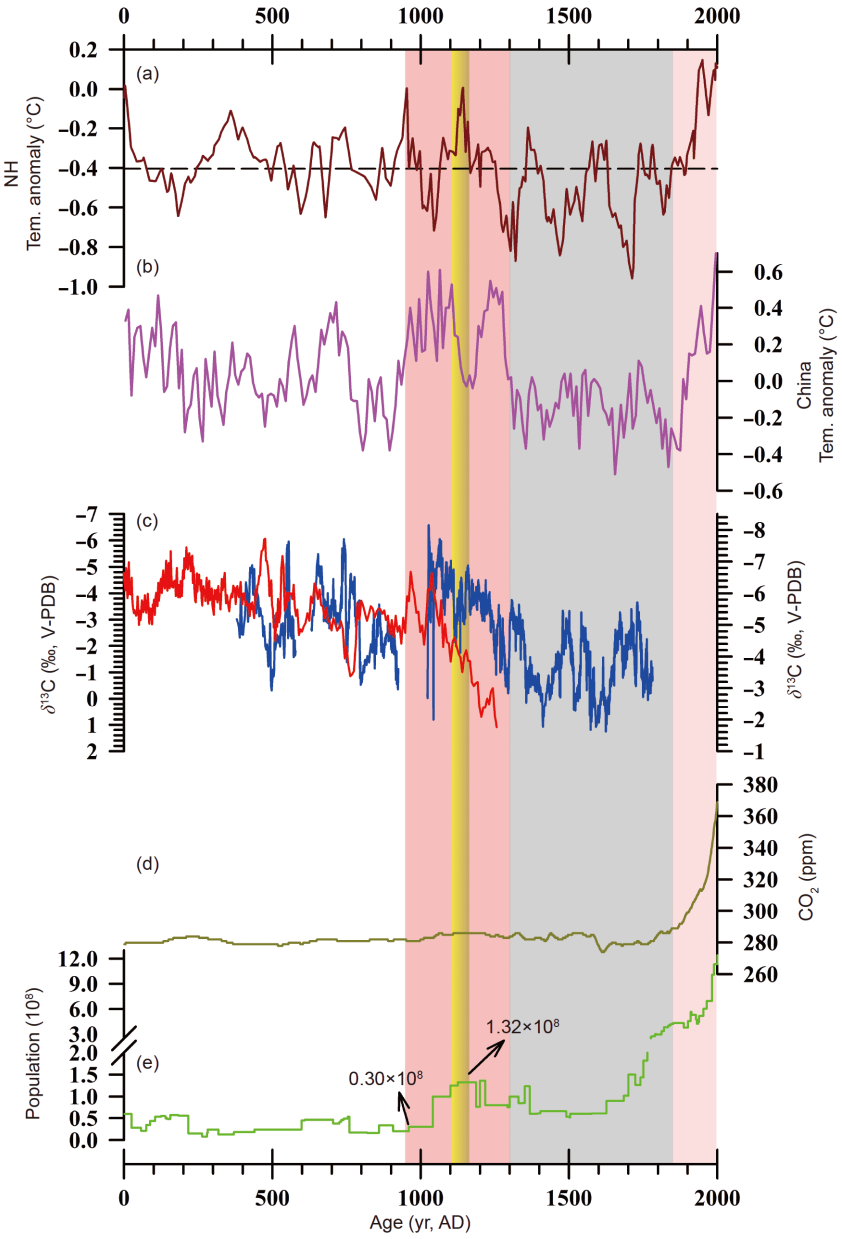

Figure 6 The mechanisms of KRD expansion in southwestern China after the JK event. (a) Temperature anomaly in the Northern Hemisphere (Kobashi et al., 2012); (b) temperature anomaly in China (Ge et al., 2013); (b) the $\delta^{13}C$ values of stalagmite SJJ7 (red curve) and stalagmite SJJ-300 (blue curve); (d) the changes in the atmospheric CO_2 concentration (Etheridge et al., 1996); (e) the change in the Chinese population over the past 2000 years (Zhao, 1988).

from the historical distribution with a larger population in the north and a smaller population in the south as the population center migrated southward (Yang, 1995; Lan, 1997). Second, the population of southwestern China increased rapidly. The massive immigration not only brought advanced production technology to this region but also required the reclaiming of a great deal of land (Zhang and Peng, 2012; Fang et al., 2015); Third, the C4 plant crops quickly replaced the native C3 plants (Li et al., 2012, 2018), and large areas of forest were cut down (Kuo et al., 2011). As a result, the ecological environment of the karst regions in southwestern China was severely damaged by anthropogenic activities during the Song and Yuan dynasties. This caused KRD expansion in this area after JK event, which was recorded by the stalagmite $\delta^{13}C$ records as continuously heavy values (Figures 3 and 6).

Since the industrial revolution, global warming and the use a massive amount of fossil fuels have led to a rapid increase in the concentration of atmospheric CO_2 (Figure 6d), which might cause the $\delta^{13}C$ of stalagmites in XY and FR Cave to become lighter in the Current Warm Period (CWP) (Figure 3c and 3d) (Li H C et al., 2011; Li et al., 2017). However, the $\delta^{13}C$ of stalagmites in ZJ Cave continued to be heavier in the CWP (Figure 3b). Compared with the area of FR and XY

Cave (Chongqing region), the area of ZJ Cave (Guizhou region) is located in the severe rocky desertification area (Figure 1). Therefore, the recovery of KRD in Chongqing may lead primarily to lighter the $\delta^{13}C$ of stalagmites in FR and XY Cave, while the continued KRD in Guizhou may lead to heavier the $\delta^{13}C$ of stalagmites in ZJ Cave in CWP.

It should be noted that the dry and wet climatic changes in northern and southern China and the regions dominated by the EASM and westerlies during the LIA are still an open question (Li et al., 2021). Due to the uncertainty in the main factors influencing the changes in stalagmite $\delta^{18}O$ values in the EASM region (Ruan et al., 2019; Liu et al., 2020; Li et al., 2021), there is a certain uncertainty in solely using stalagmite $\delta^{18}O$ records or other low resolution records to determine the dry and wet change in this region (Zhang et al., 2018). Although $\delta^{18}O$ of precipitation is affected by the factors of circulation intensity, vapor source or transportation distance on the interannual to the decadal scale, stalagmite $\delta^{18}O$ in Southwest China can indicate the dry/wet change on centennial scale (Tan et al., 2015, 2018; Yin et al., 2019). In addition, multi-proxy studies will be conducive to the accurate reconstruction of regional hydrological conditions (Zhang et al., 2018). However, regardless of whether the precipitation in southwestern China increased or decreased during the LIA, our results reveal that a very clear abrupt change (heavier) occurred in the $\delta^{13}C$ values of the stalagmite from SJJ Cave during the JK event (Figure 3a), and consistent responses were also observed in the ZJ, FR, and XY Cave stalagmite records (Figure 3b–3d) (Kuo et al., 2011; Li H C et al., 2011; Li et al., 2017). Moreover, this change occurred before the LIA and continued until about AD1700 (Figure 3), indicating that the correlation between the increase in human activity (Figure 6e) and the abrupt changes (heavier) in the $\delta^{13}C$ values of the stalagmites was very distinct regardless of whether the summer monsoon was strong or weak and how the regional precipitation changed at that time.

6. Conclusions

In this research, the high-precision dating $\delta^{13}C$ record of stalagmites were used to investigate the influence of climate change and human activities on the evolution of the ecological environment in the karst regions of southwestern China over the past 2000 years. The comparison of paleoclimate records showed the opposite changes in the hydrological environments of the southwestern region and northern of the summer monsoon region in China occurred during the MWP and LIA. The arid climatic conditions in southwestern China during the MWP induced the deterioration of the ecological environment. However, the large-scale migration of the Chinese population from the north to the south after the JK event (AD1127) and the increased human activities, such as massive deforestation and cultivated land reclamation, aggravated the KRD expansion in southwestern China. Therefore, the joint action of the climate changes and human activities may have eventually triggered the KRD expansion in the karst regions of southwestern China from the MWP to the LIA. The KRD in Chongqing area gradually recovered in CWP, but not in Guizhou area. Certainly, our reconstruction results were based on limited records, and more high-resolution multi-proxy records will be needed to evaluate the mechanisms and the area of KRD expansion in southwestern China in future research. However, our research provides a potential to reconstruct the KRD expansion in the past.

Acknowledgements *We thank professor Jiang Y J, Wang B Y, and Mao Y of Southwest University for suggestions of map. Thanks to Mr. Li Y for helping us improve our English. We would like to thank Mr. Yu X of Southwest University for providing historical documents. This work was supported by the National Natural Science Foundation of China (Grant Nos. 41772170, 42011530078), and the Fundamental Research Funds for the Central Universities, China (Grant Nos. XDJK2017A010, XDJK2020D005) to Li T Y, the Chongqing Municipal Science and Technology Commission Fellowship Fund (Grant Nos. cstc2019yszx-jcyjX0002, cstc2020yszx-jcyjX0006) to Yuan D X, and the Open Project of Guangxi Key Science and Technology Innovation Base on Karst Dynamics (Grant No. KDL & Guangxi 202003) to Li J Y. ^{230}Th dating at the High-precision Mass Spectrometry and Environment Change Laboratory (HISPEC), Taiwan University, China, was supported by the Science Vanguard Research Program of the Ministry of Science and Technology (Grant No. 108-2119-M-002-012) and the Higher Education Sprout Project of the Ministry of Education, Taiwan, China (Grant No. 108L901001) to Shen C C. This research was also Supported by the China Scholarship Council (CSC) (Grant No. 202006990068) to Chen C C.*

References

Abram N J, Wright N M, Ellis B, Dixon B C, Wurtzel J B, England M H, Ummenhofer C C, Philibosian B, Cahyarini S Y, Yu T L, Shen C C, Cheng H, Edwards R L, Heslop D. 2020. Coupling of Indo-Pacific climate variability over the last millennium. Nature, 579: 385–392

Bai X Y, Wang S J, Xiong K N. 2011. Assessing spatial-temporal evolution processes of karst rocky desertification land: Indications for restoration strategies. Land Degrad Dev, 24: 47–56

Bergel S J, Carlson P E, Larson T E, Wood C T, Johnson K R, Banner J L, Breecker D O. 2017. Constraining the subsoil carbon source to cave-air CO_2 and speleothem calcite in central Texas. Geochim Cosmochim Acta, 217: 112–127

Chen J H, Chen F H, Feng S, Huang W, Liu J B, Zhou A F. 2015. Hydroclimatic changes in China and surroundings during the Medieval Climate Anomaly and Little Ice Age: Spatial patterns and possible mechanisms. Quat Sci Rev, 107: 98–111

Cheng H, Edwards R L, Shen C C, Polyak V J, Asmerom Y, Woodhead A D J, Hellstrom J, Wang Y, Kong X, Spötl C, Wang X, Alexander Jr. C E. 2013. Improvements in ^{230}Th dating, ^{230}Th and ^{234}U half-life values, and U-Th isotopic measurements by multi-collector inductively coupled plasma mass spectrometry. Earth Planet Sci Lett, 371-372: 82–91

Cheng H, Zhang H W, Zhao J Y, Li H Y, Ning Y F, Kathayat G. 2019. Chinese stalagmite paleoclimate researches: A review and perspective. Sci China Earth Sci, 62: 1489–1513

Cheng K, Xie Y, Liu Y F, Li H J, Pan C G, Peng X J, Liu S H, Chen Q, Zhou H Y. 2019. Can speleothem $\delta^{13}C$ record vegetation changes in the East Asia summer monsoon regime? A story starting from Heinrich events recorded by speleothems from northeast Sichuan in Central

China (in Chinese). Quat Sci, 39: 837–844
Dai Q, Bie C X. 2015. The economic consequence of financial pressure: Take the change of "Jing-Kang event" in Song Dynasty as an example (in Chinese). China World Econ, 38: 173–192
Dong C L. 2015. Controlling the barbarians by the exchange of salt: A tunnel vision to the bridle policy towards ethnic groups in Southwest areas in Song Dynasty (in Chinese). Study Ethn Guangxi, 124: 135–142
Duan F C, Zhang Z Q, Wang Y, Chen J S, Liao Z B, Chen S T, Shao Q F, Zhao K. 2020. Hydrological variations in central China over the past millennium and their links to the tropical Pacific and North Atlantic oceans. Clim Past, 16: 475–485
Edwards R L, Chen J H, Wasserburg G J. 1987. ^{238}U-^{234}U-^{230}Th-^{232}Th systematics and the precise measurement of time over the past 500,000 years. Earth Planet Sci Lett, 81: 175–192
Etheridge D M, Steele L P, Langenfelds R L, Francey R J, Barnola J M, Morgan V I. 1996. Natural and anthropogenic changes in atmospheric CO_2 over the last 1000 years from air in Antarctic ice and firn. J Geophys Res, 101: 4115–4128
Fairchild I J, Smith C L, Baker A, Fuller L, Spötl C, Mattey D, McDermott F, E.I.M.F. 2006. Modification and preservation of environmental signals in speleothems. Earth-Sci Rev, 75: 105–153
Fang X Q, Su Y, Yin J, Teng J C. 2015. Transmission of climate change impacts from temperature change to grain harvests, famines and peasant uprisings in the historical China. Sci China Earth Sci, 58: 1427–1439
Fleitmann D, Burns S J, Mudelsee M, Neff U, Kramers J, Mangini A, Matter A. 2003. Holocene forcing of the Indian monsoon recorded in a stalagmite from southern Oman. Science, 300: 1737–1739
Fohlmeister J, Arps J, Spötl C, Schröder-Ritzrau A, Plessen B, Günter C, Frank N, Trüssel M. 2018. Carbon and oxygen isotope fractionation in the water-calcite-aragonite system. Geochim Cosmochim Acta, 235: 127–139
Gams I. 1991. Systems of adapting the littoral dinaric karst to agrarian land use. Acta Geogr, 31: 5–106
Ge Q S, Hao Z X, Zheng J Y, Shao X M. 2013. Temperature changes over the past 2000 yr in China and comparison with the Northern Hemisphere. Clim Past, 9: 1153–1160
Guo C Q, Zhou R, Pan L Y. 2015. Analysis of drought and flood disasters in karst area of southwest China from 1900 to 2012 (in Chinese). J Water Res Water Eng, 26: 12–15
Guo S P. 1988. Farmland reclamation in Sichuan Basin in Yuan, Ming and Qing Dynasties (in Chinese). J Chin Histor Geogr, 4: 77–108
Hercman H, Pawlak J. 2012. MOD-AGE: An age-depth model construction algorithm. Quat Geochronol, 12: 1–10
Jaffey A H, Flynn K F, Glendenin L E, Bentley W C, Essling A M. 1971. Precision Measurement of Half-Lives and Specific Activities of ^{235}U and ^{238}U. Phys Rev C, 4: 1889–1906
Jiang Z, Lian Y, Qin X. 2014. Rocky desertification in Southwest China: Impacts, causes, and restoration. Earth-Sci Rev, 132: 1–12
Kathayat G, Cheng H, Sinha A, Liang Y, Li X L, Zhang H W, Li H Y, Ning Y F, Edwards R L. 2017. The Indian monsoon variability and civilization changes in the Indian subcontinent. Sci Adv, 3: e1701296
Kobashi T, Goto-Azuma K, Box J E, Gao C C, Nakaegawa T. 2012. Causes of Greenland temperature variability over the past 4000 yr: Implications for northern Hemispheric temperature changes. Clim Past, 9: 2299–2317
Kuo T S, Liu Z Q, Li H C, Wan N J, Shen C C, Ku T L. 2011. Climate and environmental changes during the past millennium in central western Guizhou, China as recorded by Stalagmite ZJD-21. J Asian Earth Sci, 40: 1111–1120
Lan J H, Xu H, Lang Y C, Yu K K, Zhou P, Kang S G, Zhou K G, Wang X L, Wang T L, Cheng P, Yan D, Yu S Y, Che P, Ye Y, Tan L C. 2020. Dramatic weakening of the East Asian summer monsoon in northern China during the transition from the Medieval warm period to the Little ice age. Geology, 48: 307–312
Lan Y. 1997. Historical Cultural Geography in Southwest China (in Chinese). Chongqing: Southwest Normal University Press. 20–171
Li B B. 1990. The history, current situation and countermeasures of population problems in Guizhou (in Chinese). Guizhou Historical Studies, 4: 121–132
Li H C, Lee Z H, Wan N J, Shen C C, Li T Y, Yuan D X, Chen Y H. 2011. The δ^{18}O and δ^{13}C records in an aragonite stalagmite from Furong Cave, Chongqing, China: A-2000-year record of monsoonal climate. J Asian Earth Sci, 40: 1121–1130
Li J Y, Li H C, Li T Y, Mii H S, Yu T L, Shen C C, Xu X. 2017. High-resolution δ^{18}O and δ^{13}C records of an AMS ^{14}C and ^{230}Th/U dated stalagmite from Xinya Cave in Chongqing: Climate and vegetation change during the late Holocene. Quat Int, 447: 75–88
Li J Y, Li T Y. 2018. Seasonal and annual changes in soil/cave air pCO_2 and the $\delta^{13}C_{DIC}$ of cave drip water in response to changes in temperature and rainfall. Appl Geochem, 93: 94–101
Li T Y, Huang C X, Tian L, Suarez M B, Gao Y. 2018. Variation of δ^{13}C in plant-soil-cave systems in karst regions with different degrees of rocky desertification in Southwest China and implications for paleoenvironment reconstruction. J Cave Karst Stud, 80: 212–228
Li T Y, Li H C, Xiang X J, Kuo T S, Li J Y, Zhou F L, Chen H L, Peng L L. 2012. Transportation characteristics of δ^{13}C in the plants-soil-bedrock-cave system in Chongqing karst area. Sci China Earth Sci, 55: 685–694
Li T Y, Shen C C, Li H C, Li J Y, Chiang H W, Song S R, Yuan D X, Lin C D J, Gao P, Zhou L P, Wang J L, Ye M Y, Tang L L, Xie S Y. 2011. Oxygen and carbon isotopic systematics of aragonite speleothems and water in Furong Cave, Chongqing, China. Geochim Cosmochim Acta, 75: 4140–4156
Li T Y, Xiao S Y, Shen C C, Zhang J, Chen C J, Cheng H, Spötl C, Huang R, Wang T, Li J Y, Wu Y, Liu Z Q, Edwards R L, Yu T L. 2021. Little Ice Age climate changes in Southwest China from a stalagmite δ^{18}O record. Palaeogeogr Palaeoclimatol Palaeoecol, 562: 110167
Li Y, Liu Z Q, Lv X X. 2016. Temporal and spatial variation response of cave drip water under rainfall condition in rocky desertification area—A case study of Shijiangjun cave, Guizhou (in Chinese). J Southwest Univ, 38: 128–133
Li Y B, Shao J A, Yang H, Bai X Y. 2008. The relations between land use and karst rocky desertification in a typical karst area, China. Environ Geol, 57: 621–627
Liang Z X. 2004. An overview of Shu road cities and regional economics in song dynasty (in Chinese). J Southwest Univ, 30: 95–100
Liu D B, Wang Y J, Cheng H, Edwards R L, Kong X G, Li T Y. 2016. Strong coupling of centennial-scale changes of Asian monsoon and soil processes derived from stalagmite δ^{18}O and δ^{13}C records, southern China. Quat Res, 85: 333–346
Liu J B, Chen F H, Chen J H, Xia D S, Xu Q H, Wang Z L, Li Y C. 2011. Humid medieval warm period recorded by magnetic characteristics of sediments from Gonghai lake, Shanxi, north China. Chin Sci Bull, 56: 2464–2474
Liu X K, Liu J B, Chen S Q, Chen J H, Zhang X, Yan J J, Chen F H. 2020. New insights on Chinese cave δ^{18}O records and their paleoclimatic significance. Earth-Sci Rev, 207: 103216
Liu Z, Sun H, Li H, Wan N. 2011. δ^{13}C, δ^{18}O and deposition rate of tufa in Xiangshui River, SW China: Implications for land-cover change caused by climate and human impact during the late Holocene. Geol Soc London Spec Publ, 352: 85–96
Liu Z Y, Wen X Y, Brady E C, Otto-Bliesner B, Yu G, Lu H Y, Cheng H, Wang Y J, Zheng W P, Ding Y H, Edwards R L, Cheng J, Liu W, Yang H. 2014. Chinese cave records and the east Asia summer monsoon. Quat Sci Rev, 83: 115–128
Luo X L, Wang S J, Bai X Y, Tan Q, Ran C, Chen H, Xi H P, Chen F, Cao Y, Wu L H, Li H W, Zhong X. 2021. Analysis on the spatio-temporal evolution process of rocky desertification in Southwest Karst area (in Chinese). Acta Ecol Sin, 41: 680–693
Polanski S, Fallah B, Befort D J, Pras A D S, Cubasch U. 2014. Regional moisture change over India during the past Millennium: A comparison of multi-proxy reconstructions and climate model simulations. Glob Planet Change, 122: 176–185
Polyak V J, Asmerom Y. 2001. Late Holocene climate and cultural changes in the southwestern United States. Science, 294: 148–151
Ruan J Y, Zhang H Y, Cai Z Y, Yang X Q, Yin J. 2019. Regional controls

on daily to interannual variations of precipitation isotope ratios in southeast China: Implications for paleomonsoon reconstruction. Earth Planet Sci Lett, 527: 115794
Scroxton N, Burns S J, McGee D, Hardt B, Godfrey L R, Ranivoharimanana L, Faina P. 2017. Hemispherically in-phase precipitation variability over the last 1700 years in a Madagascar speleothem record. Quat Sci Rev, 164: 25–36
Shen C C, Wu C C, Cheng H, Edwards R L, Hsieh Y T, Gallet S, Chang C C, Li T Y, Lam D D, Kano A, Hori M, Spötl C. 2012. High-precision and high-resolution carbonate ^{230}Th dating by MC-ICP-MS with SEM protocols. Geochim Cosmochim Acta, 99: 71–86
Sinha A, Kathayat G, Weiss H, Li H Y, Cheng H, Reuter J, Schneider A W, Berkelhammer M, Adalı S F, Stott L D, Edwards R L. 2019. Role of climate in the rise and fall of the Neo-Assyrian Empire. Sci Adv, 5: eaax6656
Sun Q L, Liu Y, Wünnemann B, Peng Y J, Jiang X Z, Deng L J, Chen J, Li M T, Chen Z Y. 2019. Climate as a factor for Neolithic cultural collapses approximately 4000 years BP in China. Earth-Sci Rev, 197: 102915
Tan L C, Cai Y J, An Z, Cheng H, Shen C C, Breitenbach S F M, Gao Y, Edwards R L, Zhang H, Du Y. 2015. A Chinese cave links climate change, social impacts and human adaptation over the last 500 years. Sci Rep, 5: 12284
Tan L C, Cai Y J, Cheng H, Edwards L R, Lan J H, Zhang H W, Li D, Ma L, Zhao P P, Gao Y L. 2018. High resolution monsoon precipitation changes on southeastern Tibetan Plateau over the past 2300 years. Quat Sci Rev, 195: 122–132
Tan L C, Shen C C, Löwemark L, Chawchai S, Edwards R L, Cai Y, Breitenbach S F M, Cheng H, Chou Y C, Duerrast H, Partin J W, Cai W, Chabangborn A, Gao Y, Kwiecien O, Wu C C, Shi Z, Hsu H H, Wohlfarth B. 2019. Rainfall variations in central Indo-Pacific over the past 2,700 y. Proc Natl Acad Sci USA, 116: 17201–17206
Tarutani T, Clayton R N, Mayeda T K. 1969. The effect of polymorphism and magnesium substitution on oxygen isotope fractionation between calcium carbonate and water. Geochim Cosmochim Acta, 33: 987–996
Wang S J, Peng T, Liu Z H, Ni J, Chen X, Zhang X B, Liu C C. 2020. Strengthen Karst surface systematic processes research, support ecological restoration and social improvement in Karst Rocky Desertification areas in Southwest China (in Chinese). Bull Chin Acad Sci, 35: 925
Wang X F, Edwards R L, Auler A S, Cheng H, Kong X G, Wang Y, Cruz F W, Dorale J A, Chiang H W. 2017. Hydroclimate changes across the Amazon lowlands over the past 45,000 years. Nature, 541: 204–207
Wang Y J, Cheng H, Edwards R L, An Z S, Wu J Y, Shen C C, Dorale J A. 2001. A high-resolution absolute-dated late Pleistocene monsoon record from Hulu Cave, China. Science, 294: 2345–2348
Wang Y J, Cheng H, Edwards R L, He Y Q, Kong X G, An Z S, Wu J Y, Kelly M J, Dykoski C A, Li X D. 2005. The Holocene Asian monsoon: Links to solar changes and North Atlantic climate. Science, 308: 854–857
Wei Q G. 1986. Analysis on the development and status of Guizhou's historical entrance (in Chinese). Guizhou Histor Studies, 2: 11–16
Wu S D. 2000. The history of population of China: Liao, Song, Jin and Yuan Dynasties (in Chinese). Shanghai: Fudan University Press. 314–500
Wu S D. 2001. The development of population in the Southern Song Dynasty (in Chinese). J Chin Histor Studies, 4: 107–124
Yan H, Sun L G, Wang Y H, Huang W, Qiu S C, Yang C Y. 2011. A record of the southern oscillation index for the past 2,000 years from precipitation proxies. Nat Geosci, 4: 611–614
Yang Z H. 1995. China Historical Population Data and the Relavant Studies (in Chinese). Beijing: Reform Press. 761–777
Yassoglou N J. 2000. History of desertification in the European Mediterranean. In: Enne G, D'Angelo M, Zanolla C, eds. Indicators for Assessing Desertification in the Mediterranean. Proceedings of the International Seminar. University of Sassari Nucleo Ricerca Desertificazion, Sassari, Italy. 9–15
Yin J J, Li H C, Tang W, Wang Z, Mii H S, Lin Y. 2019. Rainfall variability and vegetation recovery in rocky desertification areas recorded in recently-deposited stalagmites from Guilin, South China. Quat Int, 528: 109–119
Yuan D X. 1997. Rock desertification in the subtropical karst of south China. Z Geomorphol, 108: 81–90
Yuan D X, Cheng H, Edwards R L, Dykoski C A, Kelly M J, Zhang M L, Qing J M, Lin Y S, Wang Y J, Wu J Y, Dorale J A, An Z S, Cai Y J. 2004. Timing, duration, and transitions of the Last Interglacial Asian Monsoon. Science, 304: 575–578
Zeng S, Jiang Y, Liu Z. 2016. Assessment of climate impacts on the karst-related carbon sink in SW China using MPD and GIS. Global Planet Change, 144: 171–181
Zhang G L, Zhu Y G, Shao M A. 2019. Understanding sustainability of soil and water resources in a critical zone perspective. Sci China Earth Sci, 62: 1716–1718
Zhang H B, Griffiths M L, Chiang J C H, Kong W, Wu S, Atwood A, Huang J, Cheng H, Ning Y, Xie S. 2018. East Asian hydroclimate modulated by the position of the westerlies during termination I. Science, 362: 580–583
Zhang H W, Cai Y J, Tan L C, Cheng H, Qin S, An Z S, Edwards R L, Ma L. 2015. Large variations of δ^{13}C values in stalagmites from southeastern China during historical times: Implications for anthropogenic deforestation. Boreas, 44: 511–525
Zhang M, Yuan D X, Lin Y, Qin J, Bin L, Cheng H, Edwards R L. 2004. A 6000-year high-resolution climatic record from a stalagmite in Xiangshui Cave, Guilin, China. Holocene, 14: 697–702
Zhang P Z, Cheng H, Edwards R L, Chen F H, Wang Y J, Yang X L, Liu J, Tan M, Wang X F, Liu J H, An C L, Dai Z B, Zhou J, Zhang D Z, Jia J H, Jin L Y, Johnson K R. 2008. A test of climate, sun, and culture relationships from an 1810-year Chinese cave record. Science, 322: 940–942
Zhang Q, Gemmer M, Chen J Q. 2008. Climate changes and flood/drought risk in the Yangtze delta, China, during the past millennium. Quat Int, 176-177: 62–69
Zhang S Y. 1991. A preliminary study on the natural causes of the great cyclical fluctuation of China's historical population (in Chinese). Population Res, 5: 26–31
Zhang S Y, Peng F R. 2012. On the Song dynasty population migration to the national blend promote in the Wujiang River basin (in Chinese). Guizhou Ethnic Stud, 3: 122–127
Zhang W. 2002. Reliving and setting down refugees: Practical approaches to social control in Song Dynasty (in Chinese). J Southwest Univ, 28: 124–130
Zhang W. 2004. The national conflict and social control of Southwest China in Song Dynasty (in Chinese). J Southwest Univ, 30: 102–107
Zhao K, Wang Y, Edwards R L, Cheng H, Kong X G, Liu D B, Shao Q F, Cui Y F, Huang C C, Ning Y F, Yang X L. 2020. Late Holocene monsoon precipitation changes in southern China and their linkage to Northern Hemisphere temperature. Quat Sci Rev, 232: 106191
Zhao K, Wang Y, Edwards R L, Cheng H, Liu D B, Kong X G. 2015. A high-resolved record of the Asian summer monsoon from Dongge cave, china for the past 1200 years. Quat Sci Rev, 122: 250–257
Zhao M, Li H C, Shen C C, Kang S C, Chou C Y. 2017. δ^{18}O, δ^{13}C, elemental content and depositional features of a stalagmite from Yelang Cave reflecting climate and vegetation changes since late Pleistocene in central Guizhou, China. Quat Int, 452: 102–115
Zhao W L. 1988. Chinese Population History (in Chinese). Beijing: People's Publishing House
Zheng J Y, Ge Q S, Li M Q, Zhang X Z, Liu H L, Hao Z X. 2014. Drought/flood spatial patterns in centennial cold and warm periods of the past 2000 years over eastern China. Chin Sci Bull, 59: 2964–2971

(Responsible editor: Huayu LU)